PARAMETRIX FOR THE INVERSE SOURCE PROBLEM OF THERMOACOUSTIC TOMOGRAPHY WITH REDUCED DATA

M. ELLER AND L. KUNYANSKY

Abstract. Our goal is to solve the inverse source problem of thermo- and photoacoustic tomography, with data registered on an open surface partially surrounding the source of acoustic waves. The proposed modified time reversal algorithm recovers the source term up to an infinitely smooth error term. Similarly to [1], numerical simulations show that the error term is quite small in practical terms. Unlike the latter method, the present technique is applicable in the presence of a known variable speed of sound. It is also significantly more efficient from a computational standpoint. It can be implemented using either standard finite difference techniques or through methods based on separation of variables, that for special geometries yield extremely fast image reconstruction. We illustrate our results with numerical simulations in 2 and 3 spatial dimensions.

Keywords: Thermoacoustic tomography, wave equation, wave front, parametrix, Hilbert transform

1. Introduction

We consider the inverse source problem for the free-space wave equation. This problem plays a central role in thermo- and photoacoustic tomography (TAT/PAT) [2–4], where the acoustic wave propagation is initiated by illuminating a region of interest by a short laser or microwave pulse. The energy absorbed by the biological tissues produces an instantaneous jump in the pressure due to so-called thermoelastic expansion. Customarily, detectors (e.g. hydrophones, transducers, optical interferometers) are placed on a surface completely or partially surrounding the region of interest. They measure the pressure of the outgoing acoustic wave; the goal is to recover the initial pressure from the measurements. A mathematically equivalent problem arises also in several other coupled-physics modalities (see, for example, [5–7]).

The inverse source problem for the wave equation in the free space is well understood by now in the case when the measuring surface entirely envelops the region of interest. However, in many application (of which arguably the most important is the breast imaging), the object (or body part) of interest can be surrounded by the detectors only partially. While the theoretical foundations of this problem (injectivity, stability, etc.) have been developed for this case, practical image reconstruction algorithms are a work in progress. In this paper we develop an image reconstruction procedure that recovers the initial pressure up to an infinitely smooth error term. In our numerical simulations the latter error has been quite small. Our analysis is microlocal in nature, similarly to that in our previous work [1] where the source is reconstructed by solving the exterior problem and by finding the Radon projections of that solution. However, the present approach is based on a different principle (a modified time reversal); unlike the previous technique it works with a non-uniform (but known) speed of sound, and, for general acquisition surfaces, it is much more efficient computationally.

2. Formulation of the problem

The forward problem of TAT/PAT is frequently modeled (see e.g. [8]) by the Cauchy problem for the standard wave equation in $\mathbb{R}^d$, $d \geq 2$:

$$c^2(x)\Delta u(t,x) = u_{tt}(t,x), \quad t > 0, \quad x \in \mathbb{R}^d, \tag{1}$$

with the initial condition

$$u(0,x) = f(x), \qquad u_t(0,x) = 0, \tag{2}$$

where $u(t,x)$ represents the (excess) acoustic pressure in the tissues, $c(x)$ is the speed of sound, and $f(x)$ is the initial pressure one seeks to reconstruct eventually. The function f is assumed to be supported within a bounded, closed set $\Omega_0 \subset \mathbb{R}^d$ with non-empty interior. We will assume that $c \in C^\infty(\mathbb{R}^d)$ and that $c(x)$ is constant in $\mathbb{R}^d \setminus \Omega_0$. Ideally, one would take the measurements $g(t,z)$ defined as values of $u(t,z)$ on the boundary $\partial\Omega$ of a larger open and bounded set $\Omega \supset \Omega_0$:

$$g(t,z) \equiv u(t,z), \quad z \in \partial\Omega, \quad t \in (0,\infty). \tag{3}$$

We will call such measurements full or complete. In what follows we assume that the set Ω is convex, has a smooth boundary $\partial\Omega$, and that f belongs to the Sobolev space $H^k(\mathbb{R}^d)$ with $\operatorname{supp} f \subset \Omega_0$ for some known non-negative integer k. The Sobolev space $\{f \in H^k(\mathbb{R}^d) \,:\, \operatorname{supp} f \subset \Omega_0\}$ is isomorphic to the Sobolev space $H_0^k(\Omega_0)$. The operator mapping $f(x)$ into boundary data $g(t,z)$ is continuous from $H_0^k(\Omega_0)$ into $H^k((0,\infty)\times\partial\Omega)$ [9].

Let us note, for future use, that if one extends $u(t,x)$ and $g(t,z)$ in an even fashion in t to $u^*(t,x)$ and $g^*(t,z)$ as follows

$$\begin{aligned} u^*(t,x) &= u^*(-t,x) = u(t,x), \qquad (t,x) \in [0,+\infty)\times\Omega, \\ g^*(t,z) &= g^*(-t,z) = g(t,z), \qquad (t,z) \in [0,+\infty)\times\partial\Omega, \end{aligned} \tag{4}$$

then $u^*(t,x)$ solves wave equation in $\mathbb{R}\times\Omega$ and satisfies the boundary condition $u^*(t,z) = g^*(t,z)$, $(t,z) \in \mathbb{R}\times\partial\Omega$.

2.1. **Time reversal with full data.** A useful theoretical and practical tool for recovering $f(x)$ from the boundary data g (assuming $c(x)$ is known) is time reversal. Let us define this procedure in a generalized way as follows. First, define an even $C^\infty(\mathbb{R})$ cut-off function $0 \le \kappa(s) \le 1$ such that $\kappa(s) = 1$ for $s \in [-1,1]$ and $\kappa(s) = 0$ for $|s| > m > 1$ where m is a fixed number. Now, given fixed parameters $T > 0$ and $T_1 > 0$, and some boundary conditions $h(t,z)$ defined on $(-T_1, mT)\times\partial\Omega$, one solves the following initial/boundary value problem backwards in time

$$\begin{cases} c^2(x)\Delta_x w(t,x) = w_{tt}(t,x), & (t,x) \in Q \equiv (-T_1,mT)\times\Omega, \\ w(mT,x) = 0, \qquad w_t(mT,x) = 0, & x \in \Omega, \\ w(t,z) = \kappa(Tt)h(t,z), & (t,z) \in (-T_1,mT)\times\partial\Omega. \end{cases} \tag{5}$$

This procedure defines a linear operator $\Lambda_T : h \longmapsto w$. There is a significant freedom in choosing T_1. Below we will consider both the case when T_1 is a fraction of T, and the case of T_1 being large. Furthermore we note that the extension of w by zero for all $t > mT$ preserves the wave equation in the space time cylinder $(-T_1,\infty)\times\Omega$. In particular, if $T_1 > mT$, this extension will be implied and we consider w to be defined in $(-T_1,T_1)\times\Omega$.

Let us define a restriction operator $\mathcal{R}$ that restricts a function of $(t,x) \in \mathbb{R}\times\Omega$ to its value at $t = 0$, i.e. $\mathcal{R} : w(t,x) \longmapsto w(0,x)$. We note that the composition $\mathcal{R}\Lambda_T$ is well-defined. Indeed, the operator Λ_T is a continuous operator from $H^k((-T_1,mT)\times\partial\Omega)$ into $C([-T_1,mT], H^k(\Omega)) \cap C^k([-T_1,mT], L^2(\Omega))$, for $k = 0,1,2,...$ (see [10] for $k \ge 1$ and [11] for $k = 0$) and hence, $\mathcal{R} : C([-T_1,mT], H^k(\Omega)) \to H^k(\Omega)$ is well-defined, as stated above.

Our version of the time reversal is a modification of the algorithm proposed and analyzed in [12]. The approach to this technique proposed in [9] initializes the time-reversal at $t = T$ by the harmonic extension of the boundary data (and its time derivative). This reduces the error and eliminates the necessity of the smooth cut-off. However, for the purposes of the present work the smooth cut-off proposed in [12] is preferable.

The standard time-reversal algorithm with full data is obtained when $T_1 = 0$ and boundary condition $h(t,z)$ is chosen to equal $g(t,z)$. Then, if $c(x)$ satisfies the non-trapping condition (defined below) and T is sufficiently large, the time-reversed solution $w(t,x)$ approximates $u(t,x)$ within

Q, and, in particular $w(0,x) \equiv [\mathcal{R}\Lambda_T g](x)$ coincides with $f(x)$ up to an infinitely smooth additive error term.

Moreover, in the limit $T \to \infty$ the error term vanishes and the reconstruction becomes exact [12]. In addition, in the particular case of d being odd and the speed of sound being constant (i.e. $c(x) \equiv c_0$), the reconstruction is exact for any $T \geq c_0 \operatorname{diam}(\Omega)$, because of Huygens' principle. In both cases

$$f(x) = w(0,x) = [\mathcal{R}\Lambda_T g](x), \tag{6}$$

and the time-reversed solution w coincides with the evenly extended exact solution u^*:

$$w(t,x) \equiv [\Lambda_T g^*](t,x) = u^*(t,x), \qquad (t,x) \in Q. \tag{7}$$

A variety of numerical algorithms can be utilized to solve the time reversal problem numerically. In addition to finite difference methods [13–15], under certain conditions one can also apply techniques based on eigenfunction expansions [8, 16] and even (in the presence of certain symmetries) explicit formulas similar to the method of images [17].

2.2. **Reduced data problem.** In this paper we consider the practically important case of measurements restricted to a subset Γ of $\partial\Omega$; we will call such data "reduced" and denote it by $g^{\text{reduced}}(t,z)$:

$$g^{\text{reduced}}(t,z) \equiv \begin{cases} g(t,z) = u(t,z), & z \in \Gamma \subset \partial\Omega, \\ 0, & z \in \partial\Omega \backslash \Gamma, \end{cases} \qquad t \in [0, mT]. \tag{8}$$

We will denote by $\mathfrak{A}$ the operator mapping $f(x)$ into reduced boundary data $g^{\text{reduced}}(t,z)$

$$\mathfrak{A} : f \mapsto g^{\text{reduced}}.$$

Our goal is to solve the inverse source problem with reduced data, i.e. to find $f(x)$ given $c(x)$ and $g^{\text{reduced}}(t,z)$.

2.2.1. *Theoretical foundations.* Solvability and stability of the reduced data problem have been established under the so-called visibility condition. This condition can be formulated in terms of either bicharacteristics or geometric rays for the Cauchy problem (1), (2) as follows. Since the operator is of order 2, to each $(x_0, \eta_0) \in T^*\Omega_0 \backslash 0$ there are two null bicharacteristics, denoted by $\gamma_{x_0,\eta_0,\pm}$ which are curves in $T^*\mathbb{R}^{d+1}$. They are the unique solutions to the following two initial value problems:

$$\begin{cases} \frac{dt}{ds} = \tau, \quad \frac{dx}{ds} = -c^2(x)\eta, \quad \frac{d\tau}{ds} = 0, \quad \frac{d\eta}{ds} = |\eta|^2 c(x)\nabla c(x), \\ t(0) = 0, \quad x(0) = x_0, \quad \tau(0) = \pm c(x_0)|\eta_0|, \quad \eta(0) = \eta_0. \end{cases} \tag{9}$$

Both solutions satisfy the characteristic equation $\tau^2(s) - c^2(x(s))|\eta(s)|^2 = 0$ for all s, since this relation holds for $s = 0$ and differentiating with respect to s gives

$$2\tau\frac{d\tau}{ds} - 2c(x)|\eta|^2 \left\langle \nabla c(x), \frac{dx}{ds} \right\rangle - 2c^2(x) \left\langle \eta, \frac{d\eta}{ds} \right\rangle = 2c^3(x)|\eta|^2 \langle \nabla c(x), \eta \rangle - 2c^3(x)|\eta|^2 \langle \eta, \nabla c(x) \rangle = 0 \, .$$

Here $\langle \cdot, \cdot \rangle$ denotes the scalar product in $\mathbb{R}^d$. Note that the solutions for τ are $\tau_\pm(s) = \pm c(x_0)|\eta_0|$ and hence $t_\pm(s) = \pm c(x_0)|\eta_0| s$. This allows us to use t as the parameter in each solution and write the two null bicharacteristics as

$$\gamma_{x_0,\eta_0,\pm}(t) = (t, x_\pm(t), \pm c(x_0)|\eta_0|, \eta_\pm(t)) \tag{10}$$

where $x_\pm(t)$ and $\eta_\pm(t)$ are solutions to the initial value problem

$$\dot{x}_\pm(t) = \mp c(x_\pm(t)) \frac{\eta_\pm(t)}{|\eta_\pm(t)|}, \quad \dot{\eta}_\pm(t) = \pm \nabla c(x_\pm(t))|\eta_\pm(t)|, \qquad x(0) = x_0, \quad \eta(0) = \eta_0. \tag{11}$$

The projections of the null bicharacteristics into the phase space are characteristics and denoted by $\beta_{x_0,\eta_0,\pm}(t)$, i.e. $\beta_{x_0,\eta_0,\pm}(t) = (t, x_\pm(t))$. Observe that $\beta_{x_0,\eta_0,+} = \beta_{x_0,-\eta_0,-}$.

We make the following observations.
(i) For any positive $K > 0$ we have $\beta_{x_0,\eta_0,\pm} = \beta_{x_0,K\eta_0,\pm}$.

Proof. One easily checks that if the pair $(x_\pm(t), \eta_\pm(t))$ solves (11), the pair $(x_\pm(t), K\eta_\pm(t))$ solves (11) with the last equation replaced by $\eta(0) = K\eta_0$. □

(ii) The two ODE systems (11) admit a unique solution for all $t \in \mathbb{R}$.

Proof. Compute $|\dot{x}(t)| = c(x(t))$. This gives a bound on the derivative of x over any finite time interval. Hence, there cannot be a blow-up $|x(t)| \to \infty$ at any finite time. Furthermore, since $\tau(t) = \tau(0) = \pm c(x_0)|\eta_0|$ for all t, we have $|\eta(t)| = c(x_0)|\eta_0|$ for all t. We conclude that $\eta(t)$ remains bounded for all t. □

Note that in any region where the speed of sound is constant (say equal to c_0) the system (11) can be solved explicitly and gives

$$\gamma_{x_0,\eta_0,\pm}(t) = (t, x_0 \mp c_0 t\eta_0/|\eta_0|, \pm c_0|\eta_0|, \eta_0) \quad \text{and} \quad \gamma_{x_0,-\eta_0,\pm}(t) = (t, x_0 \pm c_0 t\eta_0/|\eta_0|, \pm c_0|\eta_0|, -\eta_0)$$

for $t \in \mathbb{R}$. In particular, since we assumed that the speed of sound $c(x)$ is constant outside of Ω_0, in the compliment $\mathbb{R}^d \setminus \Omega_0$ the characteristics are straight lines.

The speed of sound satisfies the **non-trapping condition** if all characteristics $\beta_{x_0,\eta_0,\pm}$ with $(x_0, \eta_0) \in T^*\Omega_0$ satisfy $\lim_{t\to\infty} |x(t)| = \infty$.

The solvability and stability of the inverse source problem with reduced data has been established under the following

Visibility condition. [9, 18] *For the support Ω_0 of f and the measuring surface Γ, there exists number $T > 0$ such that for each $(x, \eta) \in T^*\Omega_0$ either $\beta_{x,\eta,+}$ or $\beta_{x,\eta,-}$ (or both) intersect Γ transversally for some $t \in (0, T)$.*

Moreover, this condition is necessary for the stable reconstruction of f; violating this condition makes the problem strongly ill-posed [9, 19].

2.2.2. *Known computational techniques.* We are interested in efficient computational procedures for recovering f (or a close approximation to f) from g^{reduced}, assuming that the Visibility Condition is satisfied. Let us briefly review what techniques for solving this problem are currently known. The most straightforward approach is to apply time-reversal operator $\mathcal{R}\Lambda_T$ to data g^{reduced} thus obtaining a (very) crude approximation to f. In fact, as shown in [9], the error operator $K \equiv I - \mathcal{R}\Lambda_T\mathfrak{A}$ is a pseudodifferential operator (ψDO, see [20]) of order 0 with the principal symbol bounded between 0 and 1/2. Then, one can try to approximate f by the Neumann series

$$f \approx \sum_{m=0}^{\infty} K^m \mathcal{R}\Lambda_T g^{\text{reduced}}.$$

These series converge in a microlocal sense, meaning that $f - \sum_{m=0}^{\infty} K^m \mathcal{R}\Lambda_T g^{\text{reduced}}$ is an infinitely smooth function [15]. The convergence of these series in norm has not yet been proven, although numerical experiments in the latter work have shown fast convergence.

Alternatively, one can obtain a crude approximation by defining and applying to the data the adjoint operator $\mathfrak{A}^*$ [21]. As a result, one ends up with the following integral equation with respect to f:

$$[\mathfrak{A}^*\mathfrak{A}f](x) = b(x), \qquad \text{where } b(x) \equiv \left[\mathfrak{A}^* g^{\text{reduced}}\right](x), \qquad x \in \Omega_0.$$

Since the $\mathfrak{A}^*\mathfrak{A}$ is a symmetric positive definite operator, the above equation can be solved by the conjugate gradient method [22, 23]. If there is a need to introduce a regularization, one can instead minimize

$$\|\mathfrak{A}^*\mathfrak{A}f - b\| + \text{ penalty terms},$$

where there is a choice of the norm $||\cdot||$ and penalty terms (such as, e.g., total-variation or L_2 norm of the solution) that promote needed features in the reconstructed approximation. A comparative analysis of several methods of this nature is given in [21] (see also [24]).

In spite of the obvious advantages of iterative methods, they are also relatively slow and rely on choices of regularization parameters and stopping criteria that are not always clear. Several non-iterative methods for the problem under consideration exist for the case of constant speed of sound. In particular, in [25] an explicit closed-form solution is found for the problem of recovering the Radon projections of f from g^{reduced}. Unfortunately, this technique works only under a suboptimal geometric condition resulting in the region Ω_0 being considerably smaller than the maximal region satisfying the visibility condition.

In the recent joint work of the authors with P. Hoskins [1] one recovers the Radon projections of f up to an infinitely smooth error, by solving the exterior problem for the wave equation in $\mathbb{R}^d \setminus \Omega$, and by computing the exterior Radon transform of the latter solution. This technique works only with constant $c(x) \equiv c_0$ and, with the exception of the case of a circular/spherical acquisition surface, it is quite expensive computationally.

For earlier numerical techniques for the problem with the constant speed of sound we refer the reader to [26–28].

3. Modified time reversal technique

Here we propose a new non-iterative image reconstruction procedure that, similarly to [1], reconstructs f from g^{reduced} up to an infinitely smooth additive term. Unlike the method of [1] based on solving the exterior problem, the present technique is a modification of the time reversal algorithm, and it is applicable in the case of a variable smooth speed of sound. In addition, the new method is, in general, much faster computationally. Moreover, in the case of constant speed of sound it can be efficiently implemented using eigenfunction expansions.

Since Ω_0 is closed and a subset of the open set Ω, the distance between Ω_0 and $\partial\Omega$ is $\delta > 0$. We will also consider a certain proper subset Γ_0 of Γ such that $\Gamma_0 = \{x \in \Gamma \ : \ \text{dist}(\partial\Gamma, x) > \delta_1 > 0\}$. Our method, as presented below, works subject to the following geometric condition:

Condition 1. *For the given support Ω_0 of f and subset Γ_0 of the measuring surface Γ, there exist: a choice of Cartesian coordinates, a number $T > 0$ and (arbitrarily small) $\varepsilon > 0$ such that all characteristics satisfying*

$$x(0) \in \Omega_0 \quad \text{and} \quad \dot{x}_1(t) \le 0 \quad \text{for some } |t| < \varepsilon$$

intersect the set $(0, T) \times \Gamma_0$.

Remark 1. *Due to our assumption that the speed of propagation c is constant outside of Ω_0 and the boundary of Ω is convex, if a characteristics $\beta_{x,\eta,\pm}$ with $(x, \eta) \in T^*\Omega_0$ intersects the surface $\partial\Omega$, it does so transversally. Moreover, if for some $t_0 > 0$, $x_\pm(t_0) \in \partial\Omega$, then $x_\pm(t) \in \mathbb{R}^d \setminus \Omega$ for all $t > t_0$.*

In more colloquial terms Condition 1 means that every characteristic that passes through a point in Ω_0 at $t = 0$ and that does not intersect set $(0, T) \times \Gamma_0$, must propagate to the right, i.e. in the direction of increase of $x_1(t)$, during the time interval $[-\varepsilon, \varepsilon]$ (i.e. $\dot{x}_1(t) > 0$ on interval $t \in [-\varepsilon, \varepsilon]$). Condition 1 is more restrictive than the Visibility Condition quoted above. Our additional requirement is that we specify which of the two characteristics, $\beta_{x_0,\eta_0,+}$ or $\beta_{x_0,\eta_0,-}$, should intersect the measurement surface. However, in the case of constant coefficients the two conditions can be shown to be almost equivalent ("almost" here refers to the difference between Γ_0 and Γ that can be made very small in practical terms.)

We observe that Condition 1 can be re-formulated as follows, in view of (10) and (11): If a bicharacteristic satisfies $\eta_1(t)\tau \le 0$ for some $|t| < \varepsilon$, then the corresponding characteristic intersects

$(0,T)\times\Gamma_0$ (transversally). Observe that on the complement $\partial\Omega\setminus\Gamma_0$ we have the opposite condition, i.e. the bicharacteristics intersecting $\partial\Omega\setminus\Gamma_0$ satisfy $\eta_1(t)\tau>0$ for all $|t|<\varepsilon$. The same is true for all trapped bicharacteristics, i.e. for characteristics which do not intersect $\partial\Omega$ for any time.

Condition 1 depends on the choice of the coordinate system, in particular on the choice of the coordinate x_1. From now on we assume that such choice exists and has been made, so that the latter condition is satisfied.

3.1. **Time reversal with reduced data.** When the reduced data g^{reduced} is used instead of full data g, there is a danger of creating unwanted singularities on the boundary $\partial\Gamma$. In order to avoid this we introduce a smooth spatial cut-off. To this end, define a function $\psi\in C^\infty(\partial\Omega)$ such that $0\le\psi(z)\le 1$, $\psi(z)=1$ for all $z\in\Gamma_0$ and $\psi(z)=0$ for $z\in\partial\Omega\setminus\Gamma$. We define the function $h^{\text{reduced}}\in H^k((0,\infty)\times\partial\Omega)$ by setting

$$h^{\text{reduced}}(t,z)\equiv\kappa(Tt)\psi(z)g^{\text{reduced}}(t,z)=\kappa(Tt)\psi(z)g(t,z),\qquad (t,z)\in[0,+\infty)\times\partial\Omega, \tag{12}$$

with the function $\kappa(t)$ introduced in the beginning of Section 2.1. Further, we extend $h^{\text{reduced}}(t,z)$ to negative t in an even fashion, i.e.

$$h^{\text{reduced}}(-t,z)\equiv h^{\text{reduced}}(t,z),\qquad (t,z)\in(0,+\infty)\times\partial\Omega. \tag{13}$$

Now let us consider the solution $w(t,x)$ of the time reversal problem (5) with the boundary data

$$w(t,z)=h^{\text{reduced}}(t,z),\qquad (t,z)\in(-T_1,mT)\times\partial\Omega.$$

The result is $w(t,x)\equiv\left[\Lambda_T h^{\text{reduced}}\right](t,x)$; by restricting it to $t=0$ one obtains $w(0,x)=\left[\mathcal{R}\Lambda_T h^{\text{reduced}}\right](x)$. The latter function can be viewed as a crude approximation to $f(x)$. We will call $w(0,x)$ a naïve reconstruction of $f(x)$. This approximation differs little from the one analyzed in [9], see beginning of section 2.2.2.

3.2. **Modified time reversal.** Our goal is to construct a sequence of easily computable operators that yields a microlocally accurate approximation to $f(x)$. Our method consists of applying to the time reversed solution $w(t,x)$ a linear filter that eliminates, roughly speaking, a half of all singularities contained in $w(t,x)$. Since the exact solution $u(t,x)$ satisfies the initial condition $u_t(0,x)=0$, each singularity of $f(x)$ generates two singularities of equal strength in $u(t,x)$ that propagate at $t=0^+$ in opposite directions. Each of these singularities carries full information about the corresponding singularity in $f(x)$. By eliminating one half of the singularities and by doubling the result, one can obtain a microlocally accurate approximation to $f(x)$. Some of the singularities that were present in $u(t,x)$ are absent in $w(t,x)$ since the measuring surface is open. If Condition 1 is satisfied, all the missing singularities are a subset of the singularities eliminated by our filtration procedure. Thus, they do not affect the reconstructed approximation to $f(x)$. The details are given below.

Consider the forward and inverse Fourier transforms $\mathcal{F}_n$ and $\mathcal{F}_n^{-1}$ of a function p of n variables:

$$\hat p(\xi)\equiv\left(\mathcal{F}_n p\right)(\xi)=\int\limits_{\mathbb{R}^n}p(x)e^{-i\xi\cdot x}dx,\qquad p(x)=\left(\mathcal{F}_n^{-1}\hat p\right)(x)=\frac{1}{(2\pi)^n}\int\limits_{\mathbb{R}^n}\hat p(\xi)e^{-i\xi\cdot x}d\xi,$$
$$x=(x_1,...,x_n)\in\mathbb{R}^n,\qquad \xi=(\xi_1,...,\xi_n)\in\mathbb{R}^n.$$

Further, let us define a 1-dimensional Hilbert transform $\mathcal{H}_{x_j}p$ acting along coordinate x_j, $j\in 1,...,n$:

$$\left[\mathcal{H}_{x_j}p\right](x)\equiv i\left[\mathcal{F}_n^{-1}(\hat p(\xi)\,\mathrm{sgn}(\xi_j))\right](x).$$

Note that this definition is valid as long as p is a tempered distribution, that is $p\in\mathcal{S}'(\mathbb{R}^n)$. From the definition of the Hilbert transform it follows that $\mathcal{H}_{x_j}^2=-\mathcal{I}$ and that $\mathcal{H}_{x_j}$ is a continuous operator on $H^s(\mathbb{R}^n)$. Furthermore, since the function $\mathrm{sgn}(\xi_j)$ is an odd function, we observe that the Hilbert transform maps odd functions into even ones and vice versa.

We will construct an approximation to $f(x)$ by applying a linear filter to $w(t,x)$. For a function v defined on $(-T_1,T_1)\times\Omega$ we define the extension v^0 to all of $\mathbb{R}^{d+1}$ by setting

$$v^0=\begin{cases} v & \text{for } (t,x)\in(-T_1,T_1)\times\Omega\ .\\ 0 & \text{for } (t,x)\notin(-T_1,T_1)\times\Omega\ .\end{cases}$$

We will denote the associated extension operator by $\mathcal{E}$, that is $v^0=\mathcal{E}v$. Let us introduce a smooth and symmetric cut-off in t by means of $\chi\in C_0^\infty(\mathbb{R})$ satisfying $0\le\chi\le 1$ and

$$\chi(t)=\begin{cases} 1 & \text{if } t\in(-T_1+\epsilon,T_1-\epsilon)\ ,\\ 0 & \text{if } (t,x)\notin(-T_1,T_1)\ ,\end{cases}$$

for some $\epsilon>0$. Note that $\chi w^0\in C(\mathbb{R},L^2(\mathbb{R}^d))$. Now we apply a composition of two Hilbert transforms, one with respect to t and one with respect to x_1, to χw^0 and define distribution $q(t,x)$ as follows

$$q(t,x)=[(\mathcal{I}-\mathcal{H}_{x_1}\mathcal{H}_t)(\chi w^0)](t,x),\qquad x\in\Omega,\quad t\in\mathbb{R}.$$

In fact, we are only interested in the values of q for $(t,x)\in(-\varepsilon,\varepsilon)\times\Omega_0$. Our analysis will show that the restriction to $t=0$, that is $\tilde f\equiv\mathcal{R}q$, is well defined. This is the approximate solution that we seek. (Abusing notation we denote by the same letter $\mathcal{R}$ both the restriction operator defined on $\mathbb{R}\times\mathbb{R}^d$ and the one on $\mathbb{R}\times\Omega$.) Our method is thus represented by the formula

$$\tilde f(x)\equiv[\mathcal{R}(\mathcal{I}-\mathcal{H}_{x_1}\mathcal{H}_t)(\chi w^0)](x),\qquad x\in\Omega. \tag{14}$$

Further, we observe that

$$\tilde f(x)=w(0,x)-[\mathcal{R}\mathcal{H}_{x_1}\mathcal{H}_t(\chi w^0)](x)=w(0,x)-[\mathcal{H}_{x_1}\mathcal{R}\mathcal{H}_t(\chi w^0)](x),\qquad x\in\Omega, \tag{15}$$

since operators $\mathcal{H}_{x_1}$ and $\mathcal{R}$ commute. It follows that $\tilde f(x)$ differs from $w(0,x)$ by a correction term $-[\mathcal{H}_{x_1}\mathcal{R}\mathcal{H}_t(\chi w^0)](x)$.

In the next section we show that, if Condition 1 is satisfied, the difference between $\tilde f(x)$ and $f(x)$ is a C^∞ function on Ω. Moreover, if our algorithm is applied to full data and the observation time is infinite, the reconstruction is theoretically exact.

4. Analysis of the new method

We need to make sure that formulas (14) and (15) make sense, or, more precisely, that application of the restriction operator $\mathcal{R}$ is well defined. In view of (15) it will suffice to justify the application of $\mathcal{R}$ to $\mathcal{H}_t(\chi w^0)$. This is not trivial, since when applied to a general distribution p, the one-dimensional Hilbert transform acting with respect to the variable x_j may enlarge the wave front set of p. This happens as long as there are frequencies ξ in $\mathrm{WF}(s)$ which are orthogonal to the direction of the axis x_j. More precisely we have the following result, where for convenience we set $j=n$ and abbreviate $x'=(x_1,...,x_{n-1})$:

Proposition 2. *Let $p\in\mathcal{S}'(\mathbb{R}^n)$. Then $\mathcal{H}_{x_n}p\in\mathcal{S}'(\mathbb{R}^n)$ and*

$$\mathrm{WF}(\mathcal{H}_{x_n}p)\subset\mathrm{WF}(p)\cup\{(x,\xi)\in T^*\mathbb{R}^n\ :\ (y,\xi)\in\mathrm{WF}(p),\ x'=y',\ \xi_n=0\}\ .$$

Proof. We know that

$$(\mathcal{H}_{x_n}p)(x)=\mathrm{p.v.}\frac{1}{\pi}\int_{\mathbb{R}}\frac{p(x',y_n)}{x_n-y_n}\,dy_n\ .$$

Hence, the kernel of the Hilbert transform is

$$K(x,y)=\mathrm{p.v.}\frac{1}{\pi}\frac{\delta(x'-y')}{x_n-y_n}\ .$$

Let

$$k(x)=\mathrm{p.v.}\frac{\delta(x')}{\pi x_n}=\frac{1}{\pi}\delta(x')\otimes\underline{x}_n^{-1}\qquad x'=(x_1,...,x_{n-1})\ ,$$

where $\underline{x_n^{-1}}$ is the Hörmander's notation for the principal value of $1/x_n$ [29, p.72] . At first we will show that

$$\mathrm{WF}(k) \subset \{0\} \times (\mathbb{R}^n \setminus 0) \cup \{(0, x_n; \xi', 0) \ : \ \xi' \in \mathbb{R}^{n-1} \setminus 0\}$$

Since $\mathrm{WF}(\delta) = \{(0, \xi') \ : \ \xi' \in \mathbb{R}^{n-1} \setminus 0\}$ and $\mathrm{WF}(\underline{x_n^{-1}}) = \{(0, \xi_n) \ : \ \xi_n \neq 0\}$, the implication follows from Theorem 8.2.9 [29]. Using Theorem 8.2.4 [29] gives then

$$\mathrm{WF}(K) \subset \{(x, x; \xi, -\xi) \ : \ \xi \in \mathbb{R}^n \setminus 0\} \cup \{(x, y; \xi, -\xi) \ : \ x' = y' \text{ and } \xi \in \mathbb{R}^n \setminus 0,\ \xi_n = 0\}$$

and applying Theorem 8.2.13 [29] establishes

$$\mathrm{WF}(\mathcal{H}_{x_n} p) \subset \mathrm{WF}(p) \cup \{(x, \xi) \in T^*\mathbb{R}^n \ : \ (y, \xi) \in \mathrm{WF}(p),\ x' = y',\ \xi_n = 0\} \ .$$

□

The wave front set of a functions gives a microlocal description of the set of singularities of this function. If $(x, \xi) \in \mathrm{WF}(p)$, then we refer to x as the base point and ξ as the frequency. Let us now investigate the operator $(\mathcal{I} - \mathcal{H}_{x_1}\mathcal{H}_t)$. Note that the Hilbert transform $\mathcal{H}_{x_j}$ is a Fourier multiplier; the same is true for the composition $\mathcal{H}_{x_1}\mathcal{H}_t$. To be more specific, for $p \in \mathcal{S}'(\mathbb{R}^{d+1})$ we have

$$(\mathcal{H}_{x_1}\mathcal{H}_t)p = \mathcal{F}^{-1}_{(d+1)} \left[\hat{p}(\xi)\mathrm{sgn}(\xi_0)\mathrm{sgn}(\xi_1)\right] \ ,$$

where ξ_0 is the Fourier variable dual to t, and ξ_1 is the dual to x_1. Hence,

$$(\mathcal{I} - \mathcal{H}_{x_1}\mathcal{H}_t)p = \mathcal{F}^{-1}_{(d+1)} \left[\hat{p}(\xi)(1 - \mathrm{sgn}(\xi_0\xi_1))\right] \ . \tag{16}$$

Set $x' = (x_2, ..., x_d)$. Relying on Proposition 2 and on $1 - \mathrm{sgn}(\xi_0\xi_1) = 0$ whenever $\xi_0\xi_1 > 0$, we have

$$\begin{aligned} \mathrm{WF}([\mathcal{I} - \mathcal{H}_{x_1}\mathcal{H}_t]p) \subset & [\mathrm{WF}(p) \cap \{(t, x; \xi_0, \xi) \in T^*\mathbb{R}^{d+1} \ : \ \xi_0\xi_1 \leq 0\}] \\ & \cup \{(t, x; 0, \xi) \in T^*\mathbb{R}^{d+1} \ : \ (s, x; 0, \xi) \in \mathrm{WF}(p)\} \\ & \cup \{(t, x; \xi_0, 0, \xi') \in T^*\mathbb{R}^{d+1} \ : \ (t, y; \xi_0, 0, \xi') \in \mathrm{WF}(p), x' = y'\} \\ & \cup \{(t, x; 0, 0, \xi') \in T^*\mathbb{R}^{d+1} \ : \ (s, y; 0, 0, \xi') \in \mathrm{WF}(p), x' = y'\} \ . \end{aligned} \tag{17}$$

On one hand the application of the operator $\mathcal{I} - \mathcal{H}_{x_1}\mathcal{H}_t$ will eliminate all elements of the wave front which satisfy $\xi_0\xi_1 > 0$. On the other hand, points in the wave front set with zero time frequency $\xi_0 = 0$ can produce singularities at all points on the straight line parallel to the t-axis passing through the base point. The same is true with respect to the x_1 variable. Finally, these two occurrences can be combined: If there is a point in the wave front set whose frequency satisfies $\xi_0 = \xi_1 = 0$, then the application of $\mathcal{I} - \mathcal{H}_{x_1}\mathcal{H}_t$ can spread this singularity to all points on the plane parallel to the tx_1-plane containing the base point.

The operator $(\mathcal{I} - \mathcal{H}_{x_1}\mathcal{H}_t)$ applied to χw^0 will have an impact on the wave front set. At the end of the section we will use formula (17) to understand the wave front set of $(\mathcal{I} - \mathcal{H}_{x_1}\mathcal{H}_t)\chi w^0$. Note that due to the extension by zero outside of the space time cylinder, the function χw^0 has additional singularities supported on $(-T_1, T_1) \times \partial\Omega$.

We are ready to present an interesting result given by the following

Proposition 3. *Suppose that d is odd and that the speed of sound is constant, i.e. $c(x) \equiv c_0$ and $T \geq c_0 \ \mathrm{diam}(\Omega)$, or that the speed of sound is non-trapping and $T \to \infty$. If our algorithm is applied to the full data $g^*(t, z)$ (i.e. $\tilde{f}(x)$ is computed using (15) with $w = \Lambda_T g^*$), then the reconstruction is exact: $\tilde{f}(x) = w(0, x) = f(x)$ on Ω_0.*

Proof. Since due to (6) $[\mathcal{R}\Lambda_T g^*](x) = f(x)$, it is enough to show that the correction term $\mathcal{H}_{x_1}\mathcal{R}\mathcal{H}_t(\chi w^0)$ is equal to 0 on Ω_0. Due to (7), $w = \Lambda_T g^* = u^*$ is an even function of t for each $x \in \Omega$. Since χ is symmetric in t, the function χw^0 is even in t as well. It follows that $\mathcal{H}_t\chi w^0$ is odd. Therefore, if we show that the restriction operator $\mathcal{R}$ is well defined, then the proof is complete.

Let $P = \partial_t^2 - c^2(x)\Delta$. By Theorem 18.1.28 in [30] we know that

$$\mathrm{WF}(w) \subset \mathrm{Char}\, P = \{(t,x;\xi_0,\xi) \in T^*Q \setminus 0 \ : \ \xi_0^2 = c^2(x)|\xi|^2\} \, .$$

This shows that every element in the wave front set has non-zero time frequency ξ_0 and non-zero space frequency. The multiplication by χ does not enlarge the wave front set, since χ is smooth. However, the function χw^0 may have additional elements in the wave front set over the boundary $(-T_1,T_1)\times\partial\Omega$ due the extension by zero. Since $\chi w = \chi u^*$ in Q and u^* is defined for all (t,x) we can view the χw^0 as a product of the characteristic function of the space time cylinder $\mathbb{R}\times\Omega$ with χu^*. The wave front set of this characteristic function is just the co-normal bundle of $\mathbb{R}\times\partial\Omega$. Hence, we can apply Theorem 8.2.9 [29] and obtain,

$$\begin{aligned}\mathrm{WF}(\chi w^0)\big|_{(-T_1,T_1)\times\partial\Omega} \subset &\{(t,x;\alpha+\beta) \in T^*[(-T_1,T_1)\times\partial\Omega] \setminus 0 \ : \\ &(t,x;\alpha) \in \mathrm{WF}(u^*) \text{ or } \alpha = 0 \text{ and } \beta = s\nu_x, s\in\mathbb{R}\} \, .\end{aligned}$$

According to Proposition 2 the application of $\mathcal{H}_t$ can only move elements in the wave front set with zero time frequency. In particular, the wave front set of $\mathcal{H}_t\chi w^0$ has an empty intersection with the co-normal bundle of $\{0\}\times\Omega$, that is

$$N(\{0\}\times\Omega) = \{(0,x;\xi_0,0) \ : \ x\in\Omega,\, \xi_0 \neq 0\} \, .$$

Hence, the restriction operator $\mathcal{R}$ is well-defined, see Lemma 3 in [1]. □

Remark 4. *Note that we have proved $\mathcal{R}\mathcal{H}_t\chi\mathcal{E}u^* \equiv 0$. Here $\mathcal{E}$ is the extension operator, defined in Section 3.2. This result holds for any $d \geq 2$ and for any (not necessarily constant) smooth $c(x)$.*

We, however, are mostly interested in the problem with reduced data. In this case we will show that, if Condition 1 is satisfied, then the approximation $\tilde{f}(x)$ defined by (15) satisfies $\tilde{f}(x) = f(x) + r(x)$, where $r \in C^\infty(\Omega)$. In other words a left parametrix of the operator $\mathfrak{A}$ will be constructed.

Let us represent $w(t,x) \equiv \left[\Lambda_T h^{\mathrm{reduced}}\right](t,x)$ in the form

$$w(t,x) = u^*(t,x) + e(t,x)$$

where $e(t,x) \equiv w(t,x) - u^*(t,x)$ is the difference between approximation w to u^* and the exact solution u^*. Using Proposition 3, in particular the Remark above,

$$\tilde{f}(x) = [\mathcal{R}(\mathcal{I} - \mathcal{H}_{x_1}\mathcal{H}_t)(\chi w^0)](x) = f(x) + r(x), \tag{18}$$

with

$$r(x) \equiv [\mathcal{R}(\mathcal{I} - \mathcal{H}_{x_1}\mathcal{H}_t)(\chi e^0)](x). \tag{19}$$

Theorem 5. *If Condition 1 is satisfied, then $\mathcal{R}(\mathcal{I} - \mathcal{H}_{x_1}\mathcal{H}_t)(\chi\mathcal{E}\Lambda_T)$ is a left parametrix of $\mathfrak{A}$, i.e. (18) holds with $r(x) \in C^\infty(\Omega)$.* [1]

In order to prove Theorem 5 we need to take a closer look at the wave front set of g. In what follows, the exterior unit normal field of Ω along $\partial\Omega$ is denoted by ν. Let γ_0 and γ_1 denote the trace operators, i.e. linear mappings

$$\gamma_0 : u \mapsto u\big|_{\mathbb{R}\times\partial\Omega}, \qquad \gamma_1 : u \mapsto \partial_\nu u\big|_{\mathbb{R}\times\partial\Omega}$$

Proposition 6. *Let $f \in H^s(\mathbb{R}^n)$ with $\mathrm{supp}\, f \subset \Omega_0$ for some $s \in \mathbb{R}$ and let $u \in C([0,\infty), H^s(\mathbb{R}^d))$ be the unique solution to (1)-(2). Let u^* be the even extension to all times introduced in (4) and $g^* = \gamma_0 u^* = u^*\Big|_{\mathbb{R}_+\times\partial\Omega}$. Then,*

$$\begin{aligned}\mathrm{WF}(g^*) \subset &\{\big(t, x_\pm(t); \pm c(x_0)|\eta_0|, \pm[\eta_\pm(t) - (\eta_\pm(t)\cdot\nu_{x_\pm(t)})\nu_{x_\pm(t)}]\big) \in T^*(\mathbb{R}\times\partial\Omega)\setminus 0 \ : \\ &x_\pm(t) \in \partial\Omega \text{ and } (x_0,\eta_0) \in \mathrm{WF}(f)\} \, .\end{aligned}$$

[1] Note that the application of the "rough parametrix" of [26] yields an error of limited smoothness (described by a ψDO of order -1 applied to f), whereas the error resulting from the use of our parametrix is infinitely smooth.

where $x_\pm(t)$ and $\eta_\pm(t)$ are the unique solutions to the two initial value problems (11). Furthermore, every point in $\mathrm{WF}(g^*)$ is a hyperbolic point. This is to say that $(t,y;\tau,\xi)\in\mathrm{WF}(g^*)$ implies $|\tau|>c(y)|\xi|$.

Proof. By the standard results on propagation of singularities (see e.g. [31, Section 1] or [30, Chapter 23]) we know that

$$\mathrm{WF}(u^*)\subset\{\gamma_{x,\eta,+}\cup\gamma_{x,\eta,-}\ :\ (x,\eta)\in\mathrm{WF}(f)\}\subset T^*\mathbb{R}^{d+1}_+\setminus 0 \tag{20}$$

where $\gamma_{x,\eta,\pm}$ are the bicharacteristics introduced in (10). Hence, the wave front set of the restriction of u to the boundary $\mathbb{R}_t\times\partial\Omega$ is the set

$$\mathrm{WF}(u^*\big|_{\mathbb{R}\times\partial\Omega})\subset\{\gamma_{x,\eta,+}(t)\cup\gamma_{x,\eta,-}(t)\ :\ x_\pm(t)\in\partial\Omega\text{ and }(x,\eta)\in\mathrm{WF}(f)\}$$

Note that $\mathrm{WF}(u\big|_{\mathbb{R}\times\partial\Omega})\cap N(\mathbb{R}\times\partial\Omega)=\emptyset$. Hence, using Lemma 3 in [1] we obtain the wave front set of g^* from the wave front set of u by taking the tangential projection of the spatial frequency.

For the second statement, let $(t,y;\tau,\xi)\in\mathrm{WF}(g^*)$. Then there exists a point $(t,y;\tau,\eta)\in\mathrm{WF}(u^*)$ where

$$\xi=\eta-(\eta\cdot\nu_y)\nu_y\quad\text{ and }\quad|\tau|=c(y)|\eta|\ .$$

Since all bicharacteristics originating in Ω_0 intersect $\partial\Omega$ transversally, $\eta\notin T^*_y\partial\Omega$ and thus $c(y)|\xi|<c(y)|\eta|=|\tau|$. □

Remark 7. *For the normal derivative $\gamma_1 u$ of u we have a similar result:*

$$\begin{aligned}\mathrm{WF}(\gamma_1 u)\subset\{&\big(t,x_\pm(t);\pm c(x_0)|\eta_0|,\pm[\eta_\pm(t)-(\eta_\pm(t)\cdot\nu_{x_\pm(t)})\nu_{x_\pm(t)}]\big)\in T^*(\mathbb{R}\times\partial\Omega)\setminus 0\ :\\ &x_\pm(t)\in\partial\Omega\text{ and }(x_0,\eta_0)\in\mathrm{WF}(f)\}\ .\end{aligned}$$

Proposition 8. *For $|t|<\varepsilon$ and $x\in\Omega$, the frequency variables (τ,η) of the wave front set of $e=w-u^*$ satisfies $\tau\eta_1(t)>0$. Furthermore, for $|t|<\varepsilon$, e is smooth near the boundary $\partial\Omega$.*

Proof. Since $e=w-u^*$ it is the unique solution to the backwards running Cauchy-Dirichlet problem

$$\begin{cases} c^2(x)\Delta_x e(t,x)=e_{tt}(t,x), & (t,x)\in Q=(-T_1,mT)\times\Omega,\\ e(mT,x)=-u^*(mT,x), & w_t(mT,x)=-u^*_t(mT,x), \qquad x\in\Omega,\\ e(t,z)=(\kappa(Tt)\psi(z)-1)g^*(t,z), & (t,z)\in(-T_1,mT)\times\partial\Omega,\end{cases} \tag{21}$$

and $e=-u^*$ in $(mT,T_1)\times\Omega$. The last statement is void if $T_1\le mT$.

Hence, for $|t|<\varepsilon$ the function e may incur singularities from its Cauchy data and its Dirichlet data. Note that the Cauchy data of e depend only on u^*.

Combining formula (20) with Condition 1 and the comments made right after, we know that

$$\begin{aligned}&\mathrm{WF}(u^*)\cap T^*((T,\infty)\times\Omega))\\ &\qquad\subset\{\gamma(t)\in T^*((T,\infty)\times\Omega)\ :\ x(t)\in\Omega\text{ for all }t>0\text{ and }\eta_1(t)\tau>0\text{ for all }|t|<\varepsilon\}\ .\end{aligned} \tag{22}$$

Hence, the Cauchy data of e can only cause singularities supported on such bicharacteristics γ that for $|t|<\varepsilon$ satisfy $\eta_1(t)\tau>0$ and that do not intersect the boundary $\partial\Omega$ for positive $t\in(0,T)$.

To determine the singularities of e which are caused by the singularities of the Dirichlet data $(\kappa(T\cdot)\psi-1)g^*$, we rely on the work by M. Taylor [31, Section 2] which can be summarized as follows: The singularities of the Dirichlet data at a hyperbolic point can propagate only along null bicharacteristics over these points. If $(\underline{t},\underline{x};\tau,\xi)\in T^*(\mathbb{R}\times\partial\Omega)$ is a hyperbolic point, then the two null bicharacteristics over $(\underline{t},\underline{x};\tau,\xi)$ pass through the points $(\underline{t},\underline{x};\tau,\eta^+(\underline{t}))\in T^*(\mathbb{R}\times\Omega)$ and $(\underline{t},\underline{x};\tau,\eta^-(\underline{t}))\in T^*(\mathbb{R}\times\Omega)$, respectively, where $\eta^\pm(\underline{t})=\xi\pm\nu_{\underline{x}}\sqrt{\tau^2/c(\underline{x})^2-|\xi|^2}$.

The crucial observation is here that the projection of $\eta^\pm(\underline{t})$ into $T^*_{\underline{x}}\partial\Omega$ is just ξ. While the η-component of the wave front set of u^* was projected into the cotangent bundle of $\mathbb{R}\times\partial\Omega$ in order to obtain the wave front set of the Dirichlet trace g in Proposition 6, the step taken here is the

converse one. One finds the wave front set of the solution e of a Dirichlet problem by reconstructing the null bicharacteristics over the hyperbolic points in the wave front set of $(\kappa(T\cdot)\psi - 1)g^*$.

According to the previous proposition, every point in the wave front set of $(\kappa(T\cdot)\psi - 1)g^*$ is a hyperbolic point. Since e is the solution to a backward problem in time, we consider the evolution of the solution along the decrease in time. Depending on the sign of τ one characteristic is incoming, i.e. it is leaving Q at $(\underline{t}, \underline{x})$ for decreasing values of t. The other is outgoing, i.e. it is entering Q at $(\underline{t}, \underline{x})$ for decreasing values of t. Only the latter one is of interest. (Note that the terms *incoming* and *outgoing* are commonly used with respect to the boundary $\mathbb{R} \times \partial\Omega$.)

By the previous proposition, we know that $(\kappa(T\cdot)\psi - 1)g^*$ has a singularity at $(\underline{t}, \underline{x}; \tau, \xi)$ if and only if $(x_0, \eta_0) \in \mathrm{WF}(f)$ and either $\gamma_{x_0,\eta_0,+}(\underline{t}) = (\underline{t}, \underline{x}, \tau, \eta^-(\underline{t}))$ in the case $\tau > 0$ or $\gamma_{x_0,\eta_0,-}(\underline{t}) = (\underline{t}, \underline{x}, \tau, \eta^+(\underline{t}))$ for $\tau < 0$. Those null bicharacteristics may carry singularities of e. According to Condition 1 we know that those bicharacteristics satisfy $\eta_1(t)\tau > 0$ for $|t| < \varepsilon$. Combining with formula (22), we conclude that

$$\mathrm{WF}(e) \cap T^*((-\varepsilon, \varepsilon) \times \Omega) \subset \{\gamma(t) \in T^*((-\varepsilon, \varepsilon) \times \Omega) \ : \ x(0) \in \Omega_0 \text{ and } \tau\eta_1(t) > 0\} \ .$$

Since the distance between Ω_0 and $\partial\Omega$ is $\delta > 0$, we can guarantee that e is smooth near $(-\varepsilon, \varepsilon) \times \partial\Omega$ by choosing ε sufficiently small. □

Now we can finish the proof of Theorem 5 by combining the last proposition with formula (17).

Proof. We will show that

$$\mathrm{WF}([\mathcal{I} - \mathcal{H}_{x_1}\mathcal{H}_t]\chi e) \cap T^*((-\varepsilon, \varepsilon) \times \Omega) = \emptyset \ .$$

Thus, the restriction to $t = 0$, that is $r = \mathcal{R}(\mathcal{I} - \mathcal{H}_{x_1}\mathcal{H}_t)\chi e^0$, must be smooth in Ω.

Since $\chi e^0 \in \mathcal{S}'(\mathbb{R}^{d+1})$, formula (17) is applicable to assess the wave front set of $[\mathcal{I} - \mathcal{H}_{x_1}\mathcal{H}_t]\chi e^0$. The previous proposition shows that the wave front set inside of the space time cylinder $(-T_1, T_1)\times\Omega$ is confined to bicharacteristics. Since the time frequency ξ_0 of these elements is never zero, the Hilbert transform $\mathcal{H}_t$ does not change the location of these singularities. On the other hand, elements with $\xi_1 = 0$ can get moved along lines parallel to the x_1-axis. The result of the previous proposition establishes that all singularities in $(-\varepsilon, \varepsilon) \times \Omega$ get cancelled by the application of the operator $\mathcal{I} - \mathcal{H}_{x_1}\mathcal{H}_t$.

However, there is another set of singularities located on the surface $(-T_1, T_1) \times \partial\Omega$ which are caused by the extension operator. This time we cannot argue as in the proof of Proposition 3 since e is defined only in Q and has no natural extension to the whole space. Hence, we use the formula

$$\mathrm{WF}(\chi e^0) \subset \mathrm{WF}(P\chi e^0) \cup \mathrm{Char}\, P \quad \text{where} \quad P = \frac{1}{c^2}\partial_t^2 - \Delta \ ,$$

see [30, Theorem 18.1.28] to find the singularities of χe^0 on $(-T_1, T_1) \times \partial\Omega$. For that we need to compute the distribution $P(\chi e^0)$. Let $\phi \in C_0^\infty(\mathbb{R}^{d+1})$ be a test function and denote the action of the distribution $P(\chi e^0)$ on ϕ by $\langle P(\chi e^0), \phi\rangle$. Using the definition of the distributional derivative and partial integration gives

$$\begin{aligned}\langle P(\chi e^0), \phi\rangle = \langle \chi e^0, P\phi\rangle = \int_{-T_1}^{T_1}\int_\Omega \chi e P\phi \, dxdt = \int_{-T_1+\epsilon}^{T_1-\epsilon}\int_\Omega \frac{1}{c^2}[\partial_t^2\chi e\phi + 2\partial_t\chi\partial_t e\phi] \, dtdx \\ - \int_{-T_1}^{T_1}\int_{\partial\Omega} [\chi e\partial_\nu\phi - \chi\partial_\nu\phi] \, d\sigma dt \ ,\end{aligned}$$

provided e is sufficiently smooth ($e \in H^2(Q)$ will suffice.) The formula above yields

$$P(\chi e^0) = \frac{1}{c^2}\partial_t^2\chi e + \frac{2}{c^2}\partial_t\chi\partial_t e + \gamma_0(\chi e) \otimes \delta'_{(-T_1,T_1)\times\partial\Omega} + \gamma_1(\chi e) \otimes \delta_{(-T_1,T_1)\times\partial\Omega} \ , \tag{23}$$

where γ_0, γ_1 are the previously introduced trace mappings and δ_S and δ'_S are distributions supported on a smooth surface S in $\mathbb{R}^{d+1}$ defined by

$$\langle \delta_S, \phi \rangle = \int_S \phi \, d\sigma \quad \text{and} \quad \langle \delta'_S, \phi \rangle = -\int_S \partial_\nu \phi \, d\sigma \, .$$

Note that formula (23) can be justified for less regular e by means of an approximation argument. The wave front set of these two distributions is the co-normal bundle of the surface whereas the wave front of the traces is computed as in Proposition 6 and the following remark. Hence, we can apply Theorem 8.2.9 [29] and obtain,

$$\begin{aligned} \mathrm{WF}(\chi e^0)\big|_{(-T_1,T_1)\times\partial\Omega} \subset & \{(t,x;\alpha+\beta) \in T^*[(-T_1,T_1)\times\partial\Omega] \setminus 0 \ : \\ & (t,x;\alpha) \in \mathrm{WF}(e) \text{ or } \alpha = 0 \text{ and } \beta = s\nu_x, s \in \mathbb{R}\} \, . \end{aligned} \tag{24}$$

We will explain that no elements in this set get spread into the set $(-\varepsilon,\varepsilon)\times\Omega$ by the application of $\mathcal{I} - \mathcal{H}_{x_1}\mathcal{H}_t$.

According to (17) we have to be concerned with elements with zero time frequency ξ_0 and/or zero frequency ξ_1.

(i) $\xi_0 = 0$: The points in the wave front set on the lateral boundary $(-T_1,T_1)\times\partial\Omega$ with $\xi_0 = 0$ are in the co-normal bundle of the lateral boundary, according to the formula above. These singularities can get spread along the straight line passing through the base point and parallel to the t-axis. They remain on the boundary.

(ii) $\xi_0 = \xi_1 = 0$. According the formula above, these elements are in the co-normal bundle of $(-T_1,T_1)\times\partial\Omega$ and the x_1-component of ν_x is zero. From (17) we know that these singularities can be spread to points on the plane through the base point and parallel to the tx_1-plane. Since Ω is convex, these planes are outside of the cylinder $(-T_1,T_1)\times\Omega$.

(iii) $\xi_1 = 0$: If there is an element in the wave front set with $\xi_1 = 0$, the application of $\mathcal{I} - \mathcal{H}_{x_1}\mathcal{H}_t$ may spread this singularities along straight lines through the base points and parallel to the x_1-axis. This will not matter as long as $|t| > \varepsilon$. On the other hand, by the previous proposition e is smooth near the boundary for small $|t|$. Hence, the wave front set of χe^0 will be a subset of the co-normal bundle of the boundary, for $|t| < \varepsilon$. These singularities cannot enter the space time cylinder, as discussed in the previous paragraph. □

5. Algorithmic implementation of the present technique

5.1. **Re-formulation of the method.** Recall that $w(t,x)$ is the solution of the IBVP (5) with even data h^{reduced} given by equations (12) and (13). Function $w(t,x)$ is not even in t; however it can be split into a sum of an even and odd functions $w^{\text{even}}(t,x)$ and $w^{\text{odd}}(t,x)$:

$$w(t,x) = w^{\text{odd}}(t,x) + w^{\text{even}}(t,x), \tag{25}$$

$$w^{\text{even}}(-t,x) = w^{\text{even}}(t,x), \qquad w^{\text{odd}}(-t,x) = -w^{\text{odd}}(t,x), \qquad (t,x) \in [0,T_1]\times\Omega. \tag{26}$$

Function $w^{\text{odd}}(t,x)$ is a solution of a IBVP with homogeneous boundary conditions

$$\begin{cases} c^2(x)\Delta_x w^{\text{odd}}(t,x) = w^{\text{odd}}_{tt}(t,x), & (t,x) \in (-T_1,T_1)\times\Omega, \\ w^{\text{odd}}(t,z) = 0, & (t,z) \in (-T_1,T_1)\times\partial\Omega \end{cases} ; \tag{27}$$

and it also satisfies the following Cauchy conditions at $t = 0$:

$$w^{\text{odd}}(0,x) = 0, \qquad w^{\text{odd}}_t(0,x) = w_t(0,x), \qquad x \in \Omega. \tag{28}$$

This means that given $w_t(0,x)$, function $w^{\text{odd}}(t,x)$ can be computed in $(-T_1,T_1)\times\Omega$ by solving an IBVP (27), (28) forward in time form $t = 0$ to $t = T_1$, and by applying (26).

Further, since the Hilbert transform maps even functions into odd ones, one obtains:

$$\tilde{f}(x) = w(0,x) - [\mathcal{H}_{x_1}\{\mathcal{R}\mathcal{H}_t(\chi w^{\text{odd}})\}](x), \qquad x \in \Omega_0. \tag{29}$$

5.2. **Algorithms based on finite differences.** The simplest way to implement time-reversal is by using finite difference techniques (see e.g., [13–15, 32]). This approach works especially well if the boundary passes through the nodes of the computational grid, for example, if Ω is a rectangle sampled using a Cartesian grid. Then one can use a very simple

Algorithm 1(a):

(1) Solve problem IBVP (5) backwards in time from $t = mT$ to $t = -T_1$;
(2) Compute $\tilde{f}(x)$ using (14).

For Algorithms 1(a) and 1(b) (described below), one can choose T_1 to be a small fraction of T (see section 6.2 for examples).

Using the re-formulation presented in the previous section, one arrives at the

Algorithm 1(b):

(1) Solve problem IBVP (5) backwards in time from $t = mT$ to $t = 0$;
(2) Obtain functions $w(0, x)$ and $w_t(0, x)$;
(3) Solve IBVP (27) forward in time to $t = T_1$;
(4) Extend $w^{\text{odd}}(t, x)$ to $t \in [-T_1, 0]$ using (26);
(5) Compute $\tilde{f}(x)$ using (29).

In comparison with the finite difference implementations of the method of [1], the present technique offers two advantages. First, it works with a variable speed of sound $c(x)$ (subject to Condition 1). In addition it is, in general, significantly faster. Consider, for example, a situation where Ω is a cube C with a side length a, whose interior and exterior are discretized using the same Cartesian grid defined in the whole of $\mathbb{R}^3$. Let's say the speed of sound is constant and equal c_0. For the present technique the interior problem would have to be solved in $[-T_1, mT] \times C$, with $T = c_0 a\sqrt{3}$. On the other hand, the method of [1] requires solving an exterior (with respect to C) problem in a sphere of diameter $3T$, on the time interval $[0, T]$. While the time intervals are comparable (T_1 can be chosen to be much smaller than T, and $m > 1$ can be chosen to be close to 1), the volume of the sphere is equal $\frac{9\pi T^3}{2}$ comparing to T^3 for that of the cube. In other words, the number of nodes of the Cartesian grid in the exterior of the cube C contained inside the sphere is about $(9\pi/2 - 1) \approx 13$ times larger than the number of nodes inside C. Therefore, if the same time step is used in both algorithms, the present technique requires about an order of magnitude fewer floating point operations. In addition, it eliminates the need to compute the d-dimensional Radon transform, which is very costly if done in a straightforward way.

5.3. **Algorithm based on separation of variables.** While finite difference algorithms for solving problems (5) and (27) are well known and are easy to implement, techniques based on separation of variables and/or spectral approximations of solutions offer much higher accuracies and, in certain cases, faster computations — when these techniques are applicable. In particular, separation of variables allows one to write the solution of the wave equation in Ω in terms of the eigenfunctions $\varphi_k(x)$ of the positive Dirichlet Laplacian $\Delta_{c(x)} \equiv -c^2(x)\Delta_x$, see for example [8, 16]. For completeness of the presentation we briefly (and very formally) review this known technique.

The eigenfunctions $\varphi_k(x)$ of $\Delta_{c(x)}$ are defined by the equation

$$-c^2(x)\Delta_x\varphi_k(x) = \lambda_k^2\varphi_k(x), \qquad \varphi_k(z)|_{z\in\partial\Omega} = 0, \qquad k \in \mathbb{N},$$

where the positive numbers λ_k^2 are the eigenvalues corresponding to $\varphi_k(x)$. Eigenfunctions φ_k are normalized to form a complete orthonormal system in $L^2(\Omega, c^{-2}(x))$ under the weighted inner product:

$$< \varphi_k, \varphi_m > \equiv \int_\Omega \varphi_k(x)\varphi_m(x)\frac{1}{c^2(x)}dx = 0 \text{ if } k \neq m, \qquad < \varphi_k, \varphi_k >= 1, \text{ for } k \in \mathbb{N}.$$

In order to solve problem (5) (with the boundary conditions $h^{\text{reduced}}(t,z)$) one introduces a harmonic (in x) function $H(t,x)$, that for each fixed $t \in [-T_1, mT)$ solves the Dirichlet problem in Ω subject to the boundary conditions

$$H(t,z) = h^{\text{reduced}}(t,z), \qquad (t,z) \in [-T_1, mT) \times \partial\Omega. \tag{30}$$

Then the solution $w(t,x)$ is sought in the form

$$w(t,x) = H(t,x) + \sum_k c_k(t)\varphi_k(x),$$

where time dependent coefficients $c_k(x)$ are given by the following formula

$$c_k(t) = -\frac{1}{\lambda_k}\int_t^{mT} H_k(\tau)\sin(\lambda_k(\tau - t))d\tau,$$

$$\text{with } H_k(t) \equiv \int_{\partial\Omega} h^{\text{reduced}}(t,z)\frac{\partial}{\partial\nu}\varphi_k(z)dA(z). \tag{31}$$

This yields, in particular,

$$c_k(0) = -\frac{1}{\lambda_k}\int_0^{mT} H_k(\tau)\sin(\lambda_k\tau)d\tau. \tag{32}$$

Since $\text{dist}(\Omega_0, \partial\Omega) = \delta > 0$, there is an interval $I \equiv [-\varepsilon_0, \varepsilon_0]$ such that $h^{\text{reduced}}(t,z) = 0$ for $(t,z) \in I \times \partial\Omega$. It follows that $H_k(t) = H_{tt}(t,x) = 0$ when $t \in I$, $k \in \mathbb{N}$. Therefore,

$$w(0,x) = \sum_k c_k(0)\varphi_k(x), \tag{33}$$

$$w_t(0,x) = \sum_k c_k'(0)\varphi_k(x), \tag{34}$$

$$c_k'(0) = \int_0^{mT} H_k(\tau)\cos(\lambda_k\tau)d\tau. \tag{35}$$

Now the odd part $w^{\text{odd}}(t,x)$ of the solution $w(t,x)$ can be obtained by solving the IBVP (27), with the initial condition on $w_t^{\text{odd}}(0,x)$ given by (34). Therefore $w^{\text{odd}}(t,x)$ can be represented as follows:

$$w^{\text{odd}}(t,x) = \sum_k \frac{c_k'(0)}{\lambda_k}\varphi_k(x)\sin(\lambda_k t).$$

Let us explicitly compute the term $\mathcal{H}_t(\chi w^{\text{odd}})$ entering the equation (29). Interchanging the order of summation and integration one obtains:

$$[\mathcal{H}_t(\chi w^{\text{odd}})](x) = \sum_k \frac{c_k'(0)}{\lambda_k}\varphi_k(x)\mathcal{H}_t(\chi(t)\sin(\lambda_k t)).$$

We now recall that $\chi(t)$ is supported on the interval $[-T_1, T_1]$ with T_1 free for us to vary. In particular, at the limit of large T_1 function $\mathcal{H}_t(\chi(t)\sin(\lambda_k t))$ is the distributional Hilbert transform of $\sin(\lambda_k t)$ which is equal to $\cos(\lambda_k t)$. So in the limit $T_1 \to \infty$ we obtain

$$[\mathcal{H}_t(\chi w^{\text{odd}})](x) = \sum_k \frac{c_k'(0)}{\lambda_k}\varphi_k(x)\cos(\lambda_k t)),$$

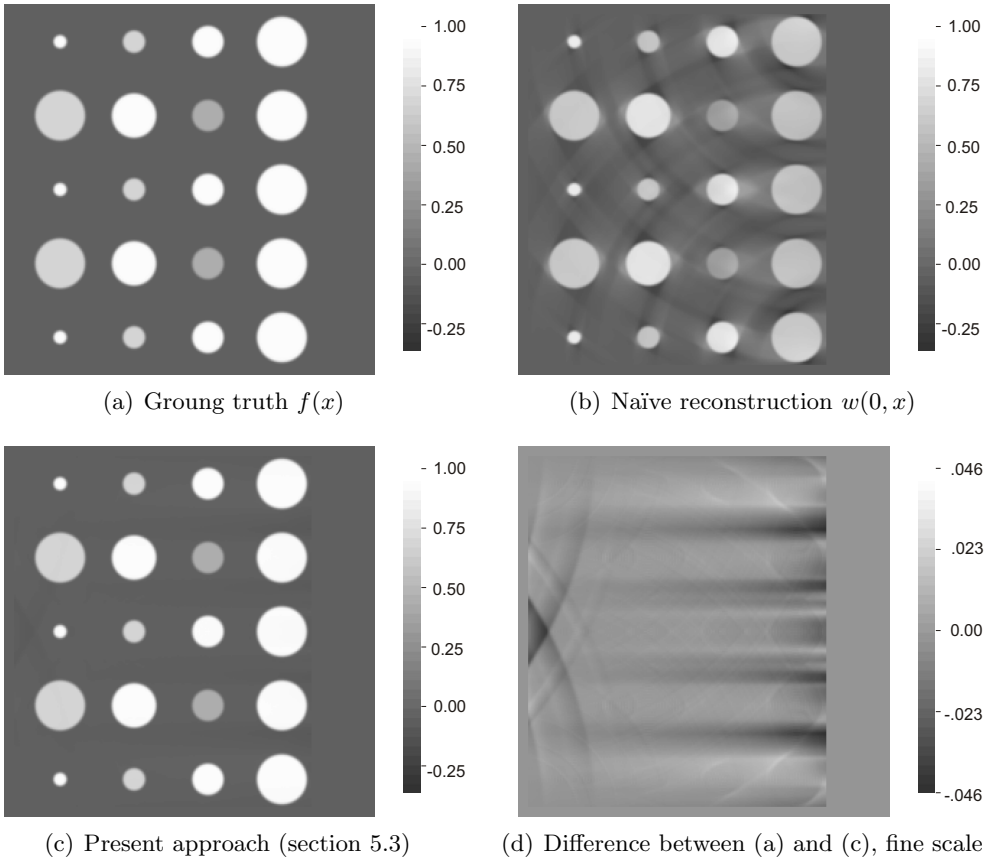

(a) Groung truth $f(x)$ (b) Naïve reconstruction $w(0,x)$

(c) Present approach (section 5.3) (d) Difference between (a) and (c), fine scale

FIGURE 1. Simulation of 3D reconstruction in a problem with a constant speed of sound

and

$$\tilde{f}(x) = w(0,x) - [\mathcal{H}_{x_1} v](x) \text{ with}$$

$$v(x) \equiv [\mathcal{R}\mathcal{H}_t(\chi w^{\text{odd}})](x) = \sum_k \frac{c_k'(0)}{\lambda_k}\varphi_k(x). \tag{36}$$

Remark 9. *As a side note, by comparing (34) and (36) one can conclude that the correction term* $[\mathcal{H}_{x_1} v](x)$ *can be expressed in terms of* $w_t(0,x)$ *as follows*

$$[\mathcal{H}_{x_1} v](x) = \left[\mathcal{H}_{x_1}\left(\Delta_{c(x)}\right)^{-\frac{1}{2}} w_t(0,\cdot)\right](x).$$

For the sake of brevity, and taking into account that the eigenfunction expansion techniques have been studied previously, we pursue here neither the proof of the above remark nor the analysis of convergence of series (34) and (35).

Assuming that the eigenfunctions φ_k are explicitly known, we arrive at the following

Algorithm 2:

(1) Compute $H_k(t)$, $k = 1, ..., M$, using (31);
(2) Compute $c_k(0)$ and $c_k'(0)$ given by (32) and (35);
(3) Compute $w(0,x)$ by summing series (33);
(4) Compute $v(x)$ by summing series (36);
(5) Compute correction term (i.e. term $\mathcal{H}_{x_1}\{\mathcal{R}\mathcal{H}_t(\chi w^{\text{odd}})\}$ in (29)) as $\mathcal{H}_{x_1}\{v(x)\}$;
(6) Compute $\tilde{f}(x)$ by adding the results of step 3 and step 5.

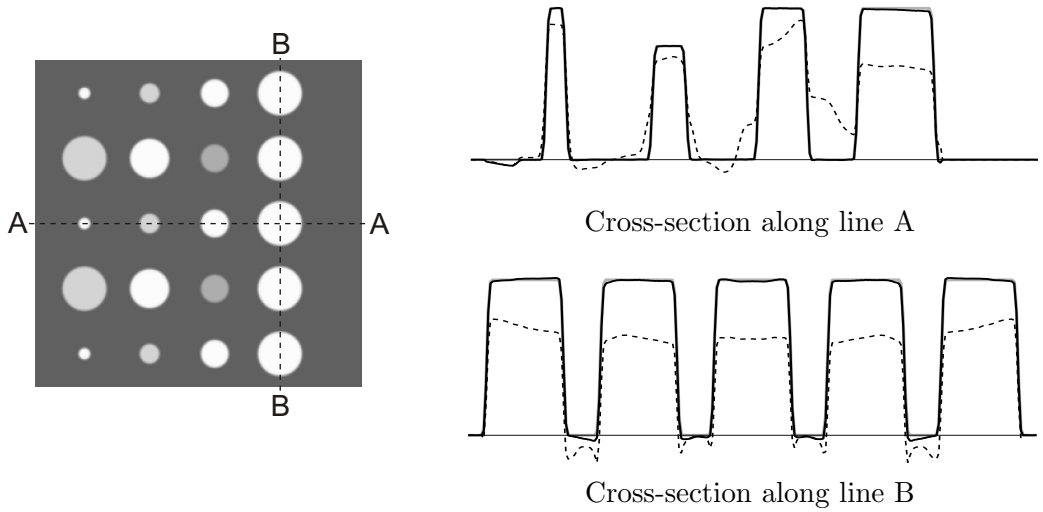

FIGURE 2. Cross sections of the 3D example. The dotted line represents the naïve reconstruction, the gray line is the ground truth, and the thick black line shows the proposed parametrix

The above procedure does not yet represent an efficient image reconstruction algorithm. First, this technique is only practical when eigenfunctions φ_k are known explicitly. This is mostly the case when $c(x)$ is constant, and when Ω is a rather simple geometrical region, such as ellipse, ellipsoid (including circles and spheres), finite cylinder, rectangle, certain tetrahedra and some crystallographic domains. Second, formulas for fast summation of series (33) and (36) are needed. Third, interpolation in frequency domain may be required when computing (32) and (35), since frequencies λ_k are in general, non-uniformly spaced, and their number is much larger (in 3D) than the number of uniformly spaced values sampled with the Nyquist step. An example of such an efficient algorithm implemented for a rectangular acquisition surface can be found in [16]. In one of the computational examples presented in the next section, we demonstrate the work of the latter technique modified to implement Algorithm 2.

6. Numerical simulations

In this section we describe several numerical simulations illustrating the work of the proposed technique. In section 6.1 we solve the 3D problem with a constant speed of sound. A couple of numerical experiments with non-uniform sound speeds in 2D are presented in section 6.2

All our simulations are done in rectangular domains, with acquisition surfaces being a part of the domain boundary. Such domains are important from the applied point of view, and are simple from a numerical standpoint. Even though our analysis covers only the case of infinitely smooth acquisition surfaces, our simulations show that the present approach works as expected in rectangular domains, too.

6.1. **Fast algorithm for a 3D rectangular acquisition surface.** We consider the inverse source problem with reduced data in a 3D setting, with a constant speed of sound $c(x) \equiv 1$ and the acquisition surface Γ being a subset of the boundary $\partial\Omega$ of the cube $\Omega = [-1, 1]^3$. More precisely, $\Gamma = \{x = (x_1, x_2, x_3) : x \in \partial\Omega \text{ and } x_1 \leq 0.8\}$. The support of the sought initial condition $f(x)$ is contained in the region $\Omega_0 = \{x = (x_1, x_2, x_3) : -0.95 < x_1 \leq 0.66, |x_k| < 0.95, k = 2, 3\}$. As a model initial condition $f(x)$ (the "ground truth") we utilized a linear combination of 20 slightly smoothed characteristic functions of balls with various centers, radii, and weights. All the centers where located on the plane $x_3 = 0$. One advantage of using such a phantom is that the solution

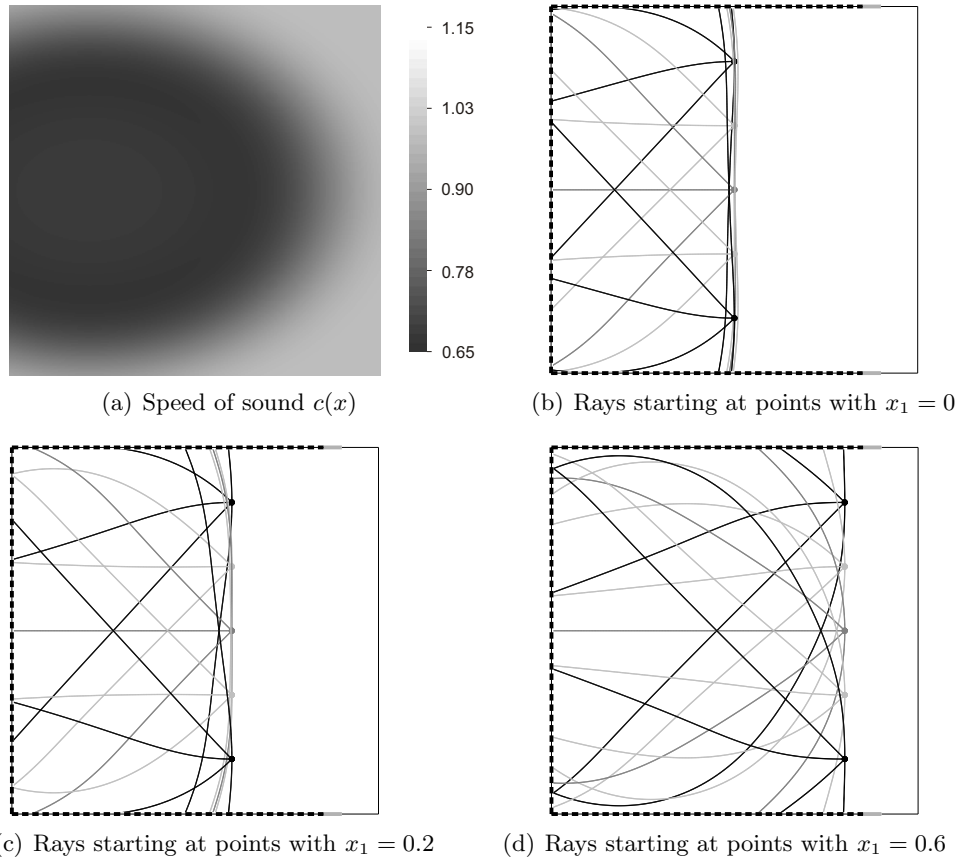

(a) Speed of sound $c(x)$ (b) Rays starting at points with $x_1 = 0$

(c) Rays starting at points with $x_1 = 0.2$ (d) Rays starting at points with $x_1 = 0.6$

FIGURE 3. Speed of sound $c(x)$ for the first 2D simulation and some of the corresponding geometric rays (characteristics). The union of the dashed line and the thick gray line is Γ

of the forward problem can be computed theoretically exactly, since the Cauchy problem with a rotationally symmetric initial conditions in 3D has an explicit solution (e.g. [33]). The gray scale representation of the restriction of $f(x)$ to the latter plane is shown in figure 1(a).

6.2. **A 2D finite difference algorithm for the problem with non-uniform speed of sound.** An asymptotically fast algorithm based on eigenfunction expansion has been developed in [16] for the problem with a rectangular acquisition surface and full data. Here we have used a modification of that algorithm along the lines of section 5.3, allowing us to compute both the naïve approximation and the correction term. The reconstructions were computed within the cube Ω discretized using a $257 \times 257 \times 257$ Cartesian grid. Computing both the naïve approximation $w(0, x)$ and the correction term took about 66 seconds of the Intel i5-6300HQ processor running at 2.3 GHz in a single-thread mode.

A central cross-section (along the plane $x_3 = 0$) of $w(0, x)$ is shown in figure 1(b); the parametrix obtained by the proposed approach is presented in the part (c) of the latter figure. While the former image clearly contains strong artifacts, the latter one looks very close to the ground truth. The relative L_∞ error in the constructed parametrix (computed over Ω_0) is 4.6%, while the relative L_2 error is about 3%. The difference between images in parts (a) and (c) can be seen in figure 1(d), where it is plotted using a much finer gray scale. In order to make the comparison more quantitative, we have drawn in figure 2 cross-sections of the images shown in figure 1 along a horizontal and a vertical line (lines A and B in figure 2). The naïve reconstruction (i.e. $w(0, x)$

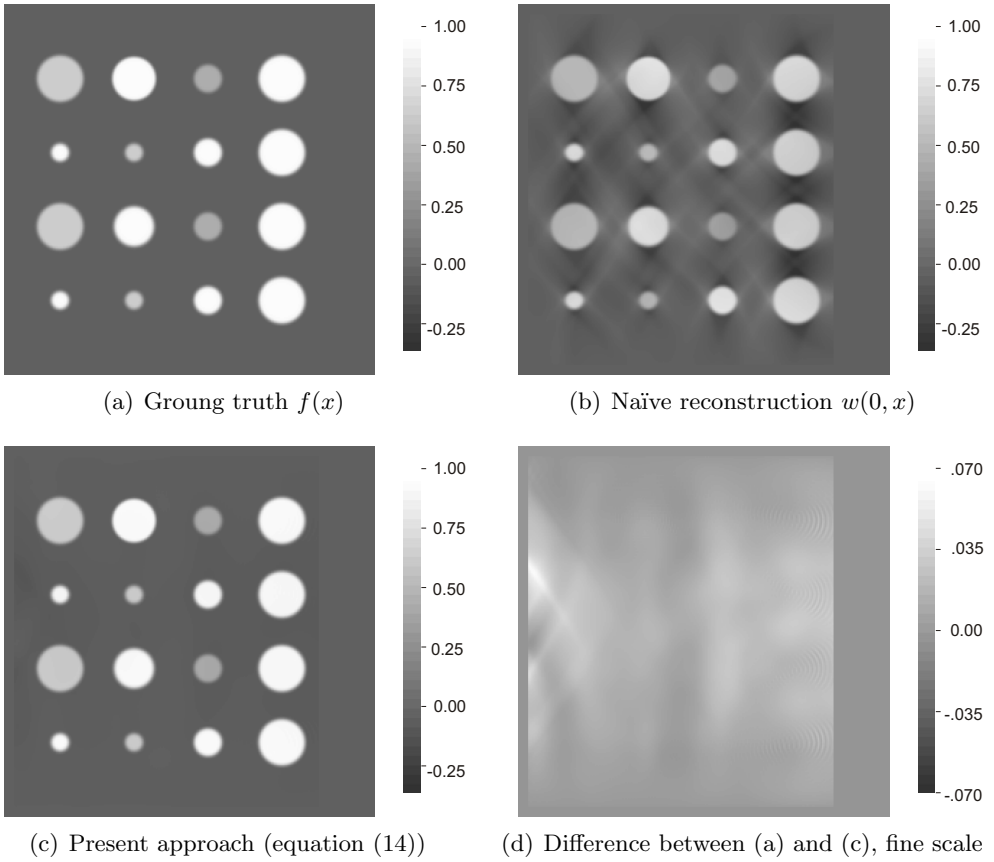

(a) Groung truth $f(x)$ (b) Naïve reconstruction $w(0,x)$

(c) Present approach (equation (14)) (d) Difference between (a) and (c), fine scale

FIGURE 4. Simulation of 2D reconstruction in a problem with a variable speed of sound

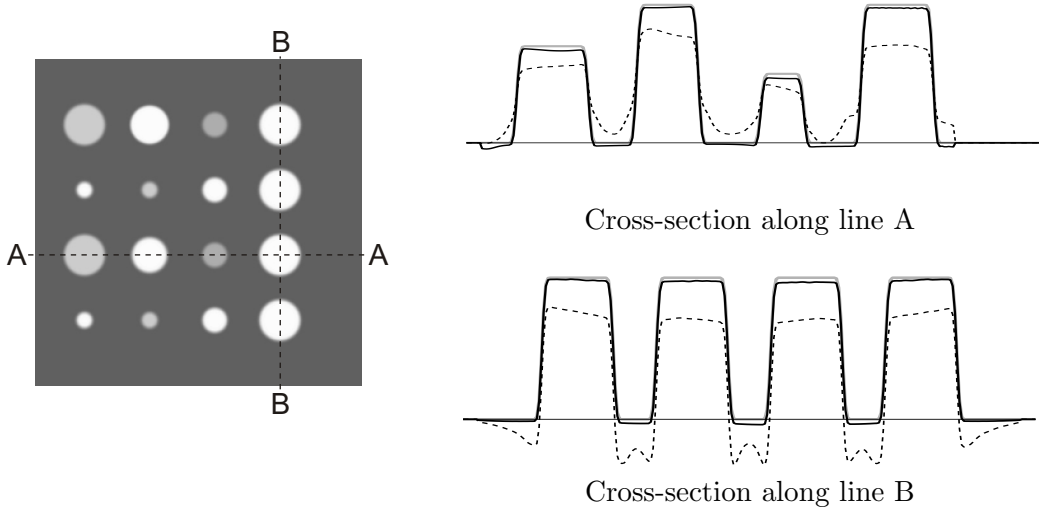

FIGURE 5. Cross-sections of the 2D example. The dotted line represents the naïve reconstruction, the gray line is the ground truth, and the thick solid black line shows the image obtained using the proposed method

computed by summing series (33)) is presented by the dashed line; the thick black line corresponds to the parametrix, and the thick gray line (partially hidden by the black line) is the ground truth.

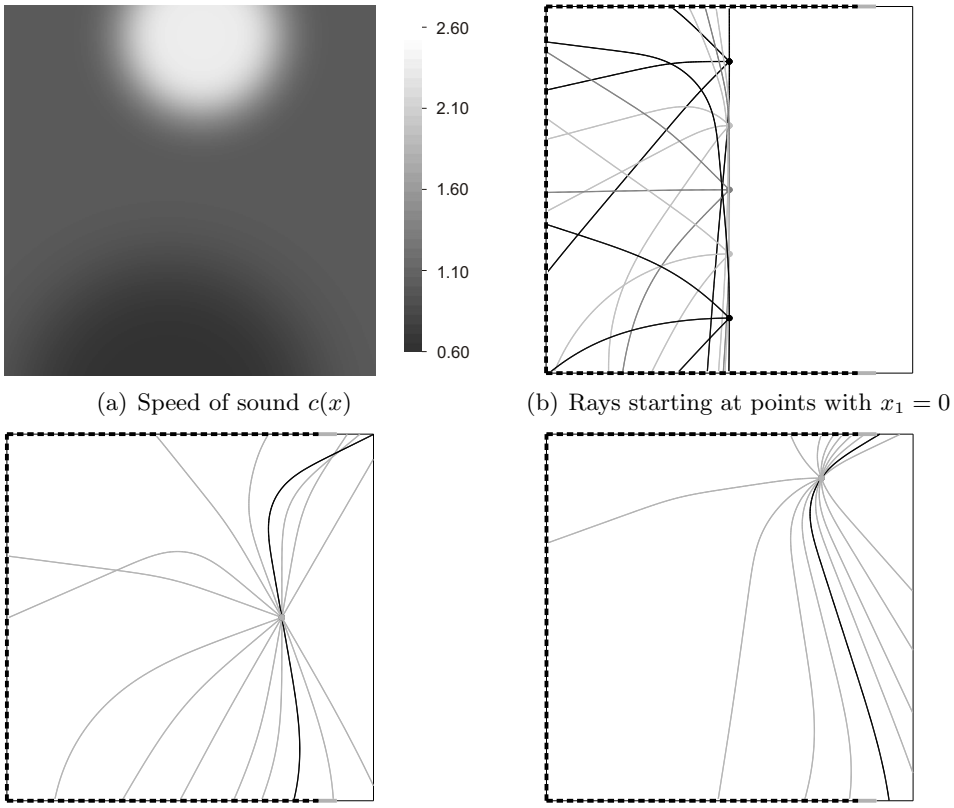

(a) Speed of sound $c(x)$

(b) Rays starting at points with $x_1 = 0$

(c) Rays starting at the point $x = (0.5, 0.0)$ Black rays do not satisfy Condition 1

(d) Rays starting at the point $x = (0.5, 0.76)$. The rays shown in black do not touch Γ

FIGURE 6. Speed of sound $c(x)$ for the second 2D simulation and some of the corresponding geometric rays (characteristics). The dashed line indicates Γ_0, and and the thick gray line is $\Gamma \setminus \Gamma_0$

In our opinion, the proposed parametrix solution, although not theoretically exact, is accurate enough for use in most practical applications.

In this section we demonstrate the work of our method in a couple of 2D simulations with variable sound speeds. In these numerical experiments the region Ω is the square $[-1, 1]^2$. The acquisition surface Γ is a subset of the boundary $\partial\Omega$, $\Gamma = \{x = (x_1,x_2)\colon\ x \in \partial\Omega \text{ and } x_1 \leq 0.8\}$. The support of the sought initial condition $f(x)$ is contained in the region $\Omega_0 = \{x = (x_1, x_2) : -0.95 < x_1 \leq 0.66, |x_2| < 0.95\}$. As the ground truth (phantom) $f(x)$ we use a linear combination of 16 slightly smoothed characteristic functions of circles with various centers, radii, and weights, see figure 4(a). Square Ω is discretized using 257×257 Cartesian grid. Both the forward problem and the time-reversal are numerically solved using the explicit finite difference algorithm resulting from applying standard second-order centered stencils in both time and space (see e.g., [34]).

For the first simulation our goal was to experiment with $c(x)$ that is significantly non-uniform and yet satisfy Condition 1. We choose the speed of sound $c(x)$ shown on a gray scale in the figure 3(a). It is can be viewed as a smooth ellipsoidal depression in a unit background, so that $0.65 \leq c(x) \leq 1$. (For convenience of numerical experimentation the support of inhomogeneity in $c(x)$ is not contained in Ω.). A variety of characteristics starting at several points with $x_1 \in \{-0.2, 0, 0.6\}$ are shown in figures 3(b)-(d), respectively. One can see that some of the characteristics are significantly bend, indicating that the effects of inhomogeneity of $c(x)$ are not negligible. The computed characteristics

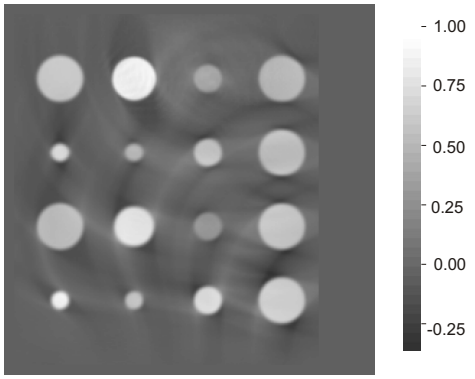

(a) Naïve reconstruction $w(0,x)$

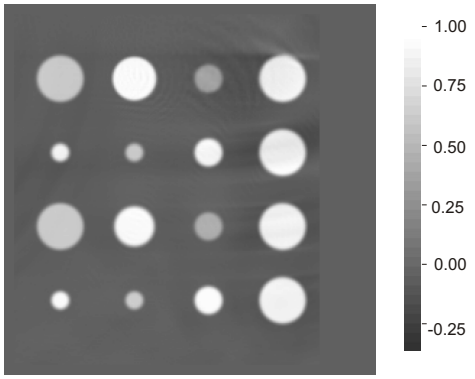

(b) Present approach (equation (14))

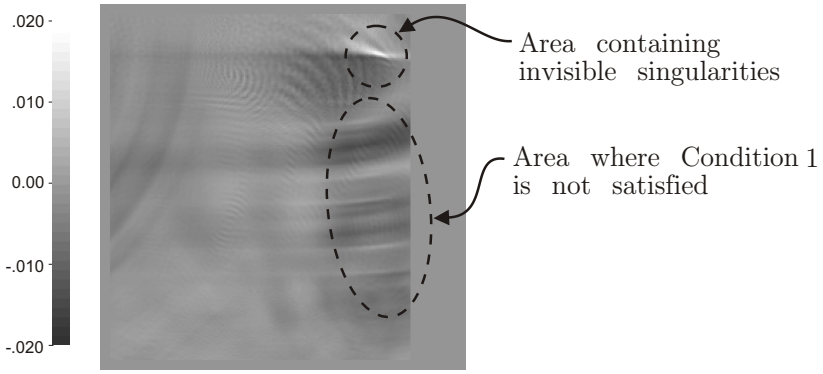

(c) Difference between (b) and the ground truth $f(x)$ shown in Figure 4(a), fine scale

FIGURE 7. Simulation of 2D reconstruction in a problem with lost rays

also satisfy Condition 1 (proving this assertion rigorously about all the needed characteristics is not easy).

In the forward problem the time step is chosen to be 0.4 times the step of the Cartesian grid (with the latter equal to 1/128). The boundary data are computed on time interval $(0, 8.5]$. The time reversal is computed from $t = mT = 8.5$ to $t = -T_1 = -0.8$, and the interval $[-0.8, 0.8]$ is used to compute the correction term, see Algorithm 1(a) in section 5.2. The result of naïve reconstruction $w(0,x)$ can be seen in the figure 4(b); the parametrix obtained by the present technique is shown in 4(c). The difference between $f(x)$ and the proposed approximation is presented in figure 4(d) on much finer gray scale. This difference (i.e., the error of reconstruction) appears smooth in accordance with our theoretical findings. The relative L_∞ norm of the error (computed over Ω_0) is 7%, while the relative L_2 error is about 6%.

In figure 5 we present cross-sections of the images shown in figures 4(a)-(c) along a horizontal and a vertical line (lines A and B in figure 5). The naïve reconstruction is given by the dashed line; the thick black line corresponds to the parametrix, and the thick gray line shows the ground truth $f(x)$.

Our second 2D numerical simulation is meant to illustrate the effects of violation of Condition 1 and the visibility condition. For this experiment we choose the speed of sound in the form of a smooth circular depression and a smooth circular bump in a unit background, as seen in figure 6(a). For this choice of $c(x)$ the maximum value is 2.46 while the minimum is 0.61. Characteristics corresponding to this sound speed are shown in figure 6(b)-(d) for a certain set of starting points and directions. Characteristics that start at points with $x_1 = 0$ (see figure 6(b)) do satisfy Condition 1.

However, for certain directions, characteristics starting at $x = (0.5, 0)$ do not satisfy the latter condition, see the black curve in figure 6(c). Namely, the ray that starts propagating "left", does not touch Γ. Meanwhile, the ray that starts propagating "right" does intersect Γ meaning that Condition 1 is violated, but the visibility condition is not. On the other hand, for a starting point $x = (0.5, 76)$ there is a pair of opposite directions such that the characteristics originating at x and going in these directions miss Γ entirely; see the black curve in the figure 6(d). It follows that the point x is "invisible". Moreover, any point lying on the black curve is "invisible".

For the forward problem the time step is chosen to be 0.15 times the step of the Cartesian grid, to guarantee stability of our numerical scheme in the presence of significantly larger (than in the previous example) speed of sound. The boundary data are calculated on time interval $(0, 8.5]$. The time reversal is computed from $t = 8.5$ to $t = -T_1 = -0.3$, and the interval $[-0.3, 0.3]$ is used to compute the correction term. The result of naïve reconstruction $w(0, x)$ can be seen in the figure 7(a); this to be compared to the ground truth $f(x)$ shown in the figure 4(a). The image produced by the proposed technique can be found in figure 7(b). The error in the latter solution (i.e. the difference with $f(x)$) is presented in figure 7(c) using a finer gray scale. A closer look at the latter figure reveals that at the regions where either visibility condition or Condition 1 is not satisfied, the error(that otherwise is supposed to be infinitely smooth) seems to develop sharp edges. In other words, our method does not produce a parametrix anymore. However, comparison of figures 7(a) and (b) suggests that even in this case the proposed technique is still a large improvement over the naïve reconstruction. Indeed, the L_2 relative error in the latter is 34% comparing to 11% in the former.

Acknowledgements The authors are grateful to the University of Lübeck for organizing the workshop "Modeling, analysis, and approximation theory toward applications in tomography and inverse problems" in June 2016 supported by the Volkswagen Foundation, that initiated their collaboration. The second author was partially supported by the NSF, award NSF/DMS 1814592. We are also thankful for anonymous referees' suggestions that helped improve this paper.

References

[1] Matthias Eller, Philip Hoskins, and Leonid Kunyansky. Microlocally accurate solution of the inverse source problem of thermoacoustic tomography. *arXiv:2004.07364*, 2020.

[2] A. A. Oraevsky, S. L. Jacques, R. O. Esenaliev, and F. K. Tittel. Laser-based optoacoustic imaging in biological tissues. *Proc. SPIE*, 2134A:122–128, 1994.

[3] R. A. Kruger, P. Liu, Y. Fang, and R. Appledorn. Photoacoustic ultrasound (PAUS) Reconstruction tomography. *Med. Phys.*, 22:1605–1610, 1995.

[4] R. A. Kruger, D. R. Reinecke, and G. A. Kruger. Thermoacoustic computed tomography - technical considerations. *Med. Phys.*, 26:1832–1837, 1999.

[5] J. Li and L. H. V. Wang. Ultrasound-modulated optical computed tomography of biological tissues. *Appl. Phys. Lett.*, 84:1597–1599, 2004.

[6] P. Kuchment and L. Kunyansky. Synthetic focusing in ultrasound modulated tomography. *Inverse Problems and Imaging*, 4:655–673, 2010.

[7] Thomas Widlak and Otmar Scherzer. Hybrid tomography for conductivity imaging. *Inverse Problems*, 28:084008, 2012.

[8] Mark Agranovsky and Peter Kuchment. Uniqueness of reconstruction and an inversion procedure for thermoacoustic and photoacoustic tomography with variable sound speed. *Inverse Problems*, 23(5):2089–2102, 2007.

[9] Plamen Stefanov and Gunther Uhlmann. Thermoacoustic tomography with variable sound speed. *Inverse Problems*, 25(7):075011, 16, 2009.

[10] Reiko Sakamoto. *Hyperbolic boundary value problems*. Cambridge University Press, Cambridge, 1982. Translated from the Japanese by Katsumi Miyahara.

[11] I. Lasiecka, J.-L. Lions, and R. Triggiani. Nonhomogeneous boundary value problems for second order hyperbolic operators. *J. Math. Pures Appl. (9)*, 65(2):149–192, 1986.

[12] Yulia Hristova. Time reversal in thermoacoustic tomography—an error estimate. *Inverse Problems*, 25(5):055008, 14, 2009.

[13] P. Burgholzer, J. Bauer-Marschallinger, H. Grün, M. Haltmeier, and G. Paltauf. Temporal back-projection algorithms for photoacoustic tomography with integrating line detectors. *Inverse Problems*, 23(6):S65–S80, 2007.

[14] Y. Hristova, P. Kuchment, and L. Nguyen. Reconstruction and time reversal in thermoacoustic tomography in acoustically homogeneous and inhomogeneous media. *Inverse Problems*, 24:055006, 2008.
[15] Jianliang Qian, Plamen Stefanov, Gunther Uhlmann, and Hongkai Zhao. An efficient Neumann series-based algorithm for thermoacoustic and photoacoustic tomography with variable sound speed. *SIAM J. Imaging Sci.*, 4(3):850–883, 2011.
[16] Leonid A. Kunyansky. A series solution and a fast algorithm for the inversion of the spherical mean Radon transform. *Inverse Problems*, 23(6):S11–S20, 2007.
[17] Leonid Kunyansky. Reconstruction of a function from its spherical (circular) means with the centers lying on the surface of certain polygons and polyhedra. *Inverse Problems*, 27(2):025012, 22, 2011.
[18] Claude Bardos, Gilles Lebeau, and Jeffrey Rauch. Sharp sufficient conditions for the observation, control, and stabilization of waves from the boundary. *SIAM J. Control Optim.*, 30(5):1024–1065, 1992.
[19] Linh V. Nguyen. On singularities and instability of reconstruction in thermoacoustic tomography. In *Tomography and inverse transport theory*, volume 559 of *Contemp. Math.*, pages 163–170. Amer. Math. Soc., Providence, RI, 2011.
[20] M. A. Shubin and S. I. Andersson. *Pseudodifferential operators and spectral theory*, volume 200. Springer, 1987.
[21] Markus Haltmeier and Linh V. Nguyen. Analysis of iterative methods in photoacoustic tomography with variable sound speed. *SIAM J. Imaging Sci.*, 10(2):751–781, 2017.
[22] M. Hanke. *Conjugate Gradient Type Methods for Ill-Posed Problems*. CRC Press, 2017.
[23] Roland Herzog and Ekkehard Sachs. Superlinear convergence of krylov subspace methods for self-adjoint problems in hilbert space. *SIAM Journal on Numerical Analysis*, 53(3):1304–1324, 2015.
[24] Kun Wang, Richard Su, Alexander A Oraevsky, and Mark A Anastasio. Investigation of iterative image reconstruction in three-dimensional optoacoustic tomography. *Physics in Medicine and Biology*, 57(17):5399–5423, aug 2012.
[25] N. Do and L. Kunyansky. Theoretically exact photoacoustic reconstruction from spatially and temporally reduced data. *Inverse Problems*, 34(9):094004, 26, 2018.
[26] D. A. Popov and D. V. Sushko. A parametrix for a problem of optical-acoustic tomography. *Doklady Mathematics*, 65(1):19–21, 2002.
[27] D. A. Popov and D. V. Sushko. Image restoration in optical-acoustic tomography. *Problemy Peredachi Informatsii*, 40(3):81–107, 2004.
[28] Leonid A. Kunyansky. Thermoacoustic tomography with detectors on an open curve: an efficient reconstruction algorithm. *Inverse Problems*, 24(5):055021, 18, 2008.
[29] Lars Hörmander. *The analysis of linear partial differential operators. I*, volume 256 of *Grundlehren der Mathematischen Wissenschaften [Fundamental Principles of Mathematical Sciences]*. Springer-Verlag, Berlin, 1983. Distribution theory and Fourier Analysis.
[30] Lars Hörmander. *The analysis of linear partial differential operators. III*, volume 274 of *Grundlehren der Mathematischen Wissenschaften [Fundamental Principles of Mathematical Sciences]*. Springer-Verlag, Berlin, 1994. Pseudo-differential operators, Corrected reprint of the 1985 original.
[31] Michael E. Taylor. Propagation, reflection, and diffraction of singularities of solutions to wave equations. *Bull. Amer. Math. Soc.*, 84(4):589–611, 1978.
[32] Peter Kuchment and Leonid Kunyansky. Mathematics of photoacoustic and thermoacoustic tomography. In *Handbook of mathematical methods in imaging. Vol. 1, 2, 3*, pages 1117–1167. Springer, New York, 2015.
[33] Markus Haltmeier, Otmar Scherzer, Peter Burgholzer, Robert Nuster, and Guenther Paltauf. Thermoacoustic tomography and the circular Radon transform: exact inversion formula. *Math. Models Methods Appl. Sci.*, 17(4):635–655, 2007.
[34] Linh V Nguyen and Leonid A Kunyansky. A dissipative time reversal technique for photoacoustic tomography in a cavity. *SIAM Journal on Imaging Sciences*, 9(2):748–769, 2016.